Atmos. Meas. Tech. Discuss., 5, 1907–1945, 2012
www.atmos-meas-tech-discuss.net/5/1907/2012/
doi:10.5194/amtd-5-1907-2012

Atmospheric Measurement Techniques Discussions

Ground-based millimeter-wave observation of stratospheric ClO over Atacama, Chile in the midlatitude Southern Hemisphere

T. Kuwahara[1], T. Nagahama[1], H. Maezawa[2], Y. Kojima[1], H. Yamamoto[3], T. Okuda[3], N. Mizuno[4], H. Nakane[5], Y. Fukui[3], and A. Mizuno[1]

[1]Solar-Terrestrial Environment Laboratory, Nagoya University, Nagoya, Aichi, Japan
[2]Department of Physics, Osaka prefecture University, Sakai, Osaka, Japan
[3]Department of Astrophysics, Nagoya University, Nagoya, Aichi, Japan
[4]National Astronomical Observatory of Japan, Mitaka, Tokyo, Japan
[5]National Insutitute for Environmental Studies, Tsukuba, Ibaraki, Japan

Received: 24 January 2012 – Accepted: 25 January 2012 – Published: 27 February 2012

Correspondence to: T. Kuwahara (kuwahara@stelab.nagoya-u.ac.jp)

Published by Copernicus Publications on behalf of the European Geosciences Union.

Abstract

We have performed ground-based measurements of stratospheric chlorine monoxide (ClO) during the summer in 2009 over the Atacama highland, Chile, a new observing site in the mid-latitude region in the Southern Hemisphere by using a millimeter-wave spectroscopic radiometer. The radiometer equipped with a superconducting receiver and a digital Fourier spectrometer is developed by Nagoya University, and the new system provides us high sensitivity and stable performance to measure the very weak ClO lines. The receiver noise temperature of the superconducting receiver is 170 K in DSB. To reveal the diurnal variation of ClO, we retrieved the vertical mixing ratio profiles by the weighted-damped least squares algorithm applied for the spectral data at 203 GHz obtained between 5 and 16 December 2009. The total error on the retrieval is estimated to be 20 % to 30 % in an altitude range from 40 to 50 km. The amplitude of the diurnal variation is ±33, ±33, and ±36 % at 40, 45, and 50 km, respectively. The time variation curve is basically similar to the previous diurnal variation observed in the northern mid-latitude region but there is a tendency that the increasing rate after the sunrise becomes smaller as the altitude increases.

1 Introduction

The chlorine chemistry plays an essential role in the ozone depletion induced by large anthropogenic input of chlorofluorocarbons (CFCs). Chlorine monoxide (ClO) is a key molecule to understand the chlorines chemistry and the ozone recovery processes (Molina and Rowland, 1974). After the enforcement of the Montreal Protocol, it is expected that the decline of ozone depleting substances (ODSs) including CFCs will lead to an increase in stratospheric ozone abundances. ClO accounts for ~25 % of the inorganic chlorine in the middle atmosphere, and the remaining ~75 % of chlorine mainly consists of HCl (Zander et al., 1996). HCl shows a significant downward trend after 1997, which is observed by the ground-based and satellite infrared measurements

AMTD
5, 1907–1945, 2012

(e.g. Rinsland et al., 2003; Mahieu et al., 2005; WMO, 2010). In WMO (2010), it is reported that the trend of stratospheric ClO has been decline at a rate of -0.9 %/yr since 1995. However, the recovery of the stratospheric ozone is not significantly discernible yet (WMO, 2010). In order to clarify the causes of the delay of the ozone recovery, further observational efforts are necessary to elucidate the trend of not only ozone but also the chlorine family (e.g., ClO) with sufficient accuracy

The long-term and short-term variations of the stratospheric ClO such as diurnal and seasonal variations are important to derive the trend of stratospheric ClO more clearly. The seasonal variations have been shown by Ricaud et al. (2000) and Nedoluha et al. (2011) based on satellite and ground-based millimeter-wave measurements. The amplitude and the shape of the diurnal variation are basic properties to derive the trend and seasonal variation especially for the molecules showing large day-and-night change like ClO, but the measurement of the diurnal variation of ClO is not so easy because of its very small spectral intensity. The first observation of diurnal variation of mid-latitude ClO over full 24-h frame was done at 287 GHz over Mauna Kea, Hawaii (Solomon et al., 1984). In 1997, Ricaud et al. showed the altitudinal difference of the ClO diurnal variation between 25 and 50 km based on the 278 GHz line observation at the Plateau de Bure, France. Ricaud et al. (2000) improved the accuracy by using the data observed AURA/MLS obtained from 1991 to 1997 within a latitude band of 40–50° N. For the polar regions, De Zafra et al. (1994), Raffalski et al. (1998), and Emmons et al. (1995) discussed the diurnal variation based on the ground-based observations from Thule in Greenland, Ny-Ålesund in Spitsbergen, and McMurdo station in Antarctica, respectively, but only Raffalski et al. (1998) presented the variation curve over 24 h. Because of the difficulty of spectroscopy of the stratospheric ClO, our current knowledge on the behavior of ClO still is not sufficient for 26 yr after the first clear evidence of the large diurnal variation obtained by Solomon et al. (1984). As seen above, the number of the observational data for ClO diurnal variation is not so large, and there was no ground-based observation from the mid-latitude region in the Southern Hemisphere.

AMTD
5, 1907–1945, 2012

This paper reports the results of the first ground-based observation of the ClO diurnal variation from the southern mid-latitude region.

First, we started the observations of vertical profiles of stratospheric minor molecules such as O_3, ClO, N_2O by using a millimeter-wave spectroscopic radiometer at Las Companas Observatory in Chile in 1999 (Mizuno et al., 2002). In August 2004, we moved and re-installed the radiometer at the Atacama highland (23° S, 68° W, alt. 4800 m). In September 2004, we started test observation of H_2O at 180 GHz band (Kuwahara et al., 2008). Then we improved the radiometer system by replacing the acousto-optical spectrometer by the digital Fourier spectrometer in 2009, and started ClO spectral observation in 204 GHz band. In this paper, we first describe the observing system and methods of observation and data reduction. Then we present the retrieval results of the vertical profile of ClO and discuss the error analysis. And finally, we discuss the ClO diurnal variation over Atacama.

2 Instrumentation and observations

2.1 Instruments

The ClO molecule has rotational transition lines in the millimeter wavelength and the rotational level splits further by the Λ-doubling and the hyperfine structure of the magnetic and the nuclear quadruple terms (e.g. Amano et al., 1985). In this study, we observed $J = 11/2 - 9/2$ lines around 204.346 GHz by upgrading the millimeter-wave heterodyne spectroscopic radiometer developed by Nagoya University and ULVAC Inc (Mizuno et al., 2002).

Figure 1 shows the block diagram of the radiometer. The radiometer consists of the quasi-optical system, the heterodyne receiver system, and the spectrometer.

For the quasi-optical system, we employed an offset-Gregorian telescope optics consisting of a paraboloidal mirror and a ellipsoidal mirror. The 10.5 cm diameter paraboloidal mirror forms a beam with a size of 1.0° in the full width at half maximum

AMTD
5, 1907–1945, 2012

(FWHM) at 204 GHz, and the beam direction i.e. the observing elevation angle is changed by the flat rotating mirror placed in front of the paraboloidal mirror. Path Length Modulator (PLM) is installed around the beam-waist between the parabolic mirror. The PLM consists of a pair of roof-top mirror, and it smooths and reduces the standing waves that cause an artificial spectral baseline ripple by periodically changing the optical path length of the optics.

The receiver frontend is a superconductor-insulator-superconducter (SIS) mixer (see e.g. Tucker and Feldman, 1985, for more details) operated in double sideband mode (DSB). The SIS mixer and the following high electron mobility transistor (HEMT) amplifier is cryogenically cooled down to ∼4 K by a closed cycle Helium mechanical refrigerator. The equivalent receiver noise temperature of the SIS mixer was 170 K in DSB at 204.546 GHz. The IF output from the SIS mixer at 2.1 GHz is processed by the room temperature IF circuits to adjust the frequency and amplitude level appropriate for the backend spectrometer.

The backend spectrometer was acousto-optical spectrometer (AOS) in the original radiometer system (Mizuno et al., 2002), but we replaced the spectrometer with new digital FFT spectrometer. Since the atmospheric pressure at the Atacama highland is about a half of that at the sea level, the cooling efficiency for the electronic devices is reduced by factor of two. Thus we put additional cooling mechanism to the original commercial FFT spectrometer to secure stability even at Atacama. The FFT spectrometer provides a bandwidth and a frequency resolution of 1 GHz and 70 kHz, respectively, and the stability of the spectrometer evaluated by Allan minimum time is ∼1000 s, improved by more than an order of magnitude compared with the previous AOS.

2.2 Observation period and site

We observed the stratospheric ClO from December 2009 to January 2010 at Nagoya University Atacama Atmospheric observing station (NATAOS) in Chile. The altitude of the station is 4800 m a.s.l. It's low water vapor pressure condition provides a very small

AMTD
5, 1907–1945, 2012

atmospheric opacity in the millimeter wavelength because the tropospheric water vapor is the major agent of absorption of stratospheric molecular spectral emission. Atacama highland is one of the best sites to observe very weak stratospheric molecular lines from the ground. Typical optical depth around 204 GHz at Atacama is less than 0.1 during the observing period.

2.3 Observation method

The ClO spectral lines were obtained by using the elevation switching method (Mizuno et al., 2002). In the elevation switching method, two different sky directions at high and low elevations are alternately observed, and the sky opacity and the receiver fluctuations are compensated by subtracting the high-elevation signal from the low-elevation signal. The high elevation angle is fixed near the zenith, and we call this angle as the reference angle. While the low elevation angle is variable along with the sky condition, and this angle is called as the observing-sky angle.

Since the contributions of the continuum emission from the lower atmosphere are different between the high and low elevations because of the difference of the air mass along the two line of sights, a lossy dielectric plate is inserted in the reference beam to equalize the continuum signal levels. However, the air mass changes with time by the sky condition, and fine tuning of the level equalization is done by the adjustment of the observing-sky angle.

Atmospheric gas or more generally translucent medium like the lossy dielectric plates do not only absorb the incident radiation but also radiate the thermal emission simultaneously. The absorption coefficient is given by $\exp(-\tau)$ and the thermal radiation intensity is expressed as $T(1-\exp(-\tau))$ in terms of the temperature (T) and the optical depth (τ) of the translucent medium.

In this study, as commonly used in the millimeter-wave spectroscopy, the radiation intensity is expressed as a brightness temperature or an equivalent temperature of blackbody that emits the same amount of radiation energy at the observing frequency. In the millimeter wavelength, the intensity is almost proportional to the blackbody temperature

AMTD
5, 1907–1945, 2012

due to the Rayleigh-Jeans raw of radiation. The output power of the receiver system, P_{out}, is proportional to the input signal power of T_{in}, and it is expressed by using a proportional coefficient, α as,

$$P_{out} = \alpha T_{out} = \alpha(T_{in} + T_{sys}) \quad (1)$$

where T_{sys} is an additional system noise generated in the receiver system. Thus the observed intensity for the reference sky, T_{ref} at the reference elevation angle, El_{ref} is written as

$$T_{ref} = \frac{T_{line}}{\sin El_{ref}} \exp\left[-\frac{\tau}{\sin El_{ref}} - \tau_{plate}\right] + T_{trop}\left[1 - \exp\left(-\frac{\tau}{\sin El_{ref}}\right)\right]\exp\left(-\tau_{plate}\right) + T_{plate}[1 - \exp(-\tau_{plate})] + T_{sys} \quad (2)$$

where T_{line} is the intensity of the stratospheric molecular emission line toward the zenith, T_{trop} is the equivalent temperature of atmosphere below the stratosphere, τ_{plate} is the optical depth of the lossy dielectric plate, and τ is the optical depth of atmosphere below the stratosphere. The intensity for the observing observing-sky, T_{obs}, is given in the same manner,

$$T_{obs} = \frac{T_{line}}{\sin El_{obs}} \exp\left[-\frac{\tau}{\sin El_{obs}}\right] + T_{trop}\left[1 - \exp\left(-\frac{\tau}{\sin El_{obs}}\right)\right] + T_{sys} \quad (3)$$

where El_{obs} is the observing-sky angle. The El_{obs} is automatically adjusted to meet the condition that T_{ref} and T_{obs} are balanced at the outside of the molecular line frequency where T_{line} is negligibly small, i.e.

$$T_{trop}\left[1 - \exp\left(-\frac{\tau}{\sin El_{ref}}\right)\right]\exp\left(-\tau_{plate}\right) + T_{plate}[1 - \exp(-\tau_{plate})] \approx T_{trop}\left[1 - \exp\left(-\frac{\tau}{\sin El_{obs}}\right)\right]. \quad (4)$$

And eventually, we have to determine the proportional coefficient α empirically to obtain the intensity scale of brightness temperature from the actual measured quantities,

AMTD
5, 1907–1945, 2012

the receiver output power. The determination of α is made by measurements of two reference blackbodies at different physical temperatures, T_{hot} and T_{cold}. α is expressed in terms of the output powers from the hot and cold blackbodies, P_{hot} and P_{cold}, as follows,

$$P_{hot} = \alpha(T_{hot} + T_{sys}) \quad (5)$$

$$P_{cold} = \alpha(T_{cold} + T_{sys}) \quad (6)$$

$$\alpha = \frac{P_{hot} - P_{cold}}{T_{hot} - T_{cold}} \quad (7)$$

The optical depth of tropospheric absorbing layer, τ, is derived by using so-called "sky tipping" procedure (Ulich et al., 1980). We measured τ every 10 min. Finally, the brightness temperature of the stratospheric ClO, T_{line} is derived from the observed quantities, P_{ref} and P_{ref} as,

$$T_{line} = \left[\frac{T_{hot} - T_{cold}}{P_{hot} - P_{cold}}(P_{obs} - P_{ref}) + T_{trop} \times \left(\exp\left(-\frac{\tau}{\sin El_{obs}}\right) - \exp\left(-\frac{\tau}{\sin El_{ref}} - \tau_{plate}\right)\right)\right] \Bigg/ \left(\frac{1}{\sin El_{obs}}\exp\left(-\frac{\tau}{\sin El_{obs}}\right) - \frac{1}{\sin El_{ref}}\exp\left(-\frac{\tau}{\sin El_{ref}} - \tau_{plate}\right)\right). \quad (8)$$

The hot reference is the room temperature radio absorber, i.e. $T_{hot} = 300$ K, and cold reference is the absorber soaked in liquid nitrogen, i.e. $T_{cold} \sim 73$ K at an altitude of 4800 m.

On the other hand, the optical depth of the lossy dielectric plate, τ_{plate}, is estimated from the Eqs. (2) and (3) by assuming $T_{trop} = T_{plate}$ as

$$\tau_{plate} = \tau\left(\frac{1}{\sin El_{obs}} - \frac{1}{\sin El_{ref}}\right). \quad (9)$$

AMTD
5, 1907–1945, 2012

We used acrylic plates with thicknesses of 1 and 5 mm in the present measurements, and the corresponding τ_{plate} are estimated to be 0.04 and 0.3, respectively. These plates were changed manually along with the sky condition, and the observing-sky angle was set within a range between 15° and 45°.

3 Data analysis

3.1 Data selection

To study the diurnal variation of the stratospheric ClO, we divided the dataset into the 3-h bins by the local time (LT) and averaged the spectral data to improve the signal-to-noise ratio. Although the channel-to-channel random noise can be reduced by the averaging, artificial features of spectral baseline cannot be reduced and remain sometimes. Baseline ripples caused by standing waves in the optical system and residuals due to the incomplete subtraction of the continuum level in the elevation-switching are considered to be the origins of such artificial features. Such features appear more significantly when the sky conditions are bad, since the line signal intensity becomes smaller relative to the features because of the large absorption. Thus first of all, we selected the data obtained in good observing condition.

Figure 2 shows the time variation of the sky optical depth over the observed period from 1 December 2009 to 17 January 2010. Even in the Atacama highland, the water vapor pressure increases in a part of the summer, that is so-called Bolivian Winter. In 2009, the Bolivian Winter seems to have started around 17 December and after that, the sky optical depth abruptly increased. on the other hand, before 5 December the sky optical depth was a little bad. Thus, we decided to concentrate the analysis for the data obtained from 5–16 December. In addition, we excluded the data obtained with an optical depth (τ) larger than 0.15 and a balanced observing-sky angle is smaller than 15° or larger than 25° for the average. The lower elevation limit is set to avoid the contamination of thermal radiation from the ground coming into through the sidelobe of

AMTD
5, 1907–1945, 2012

the telescope beam. The upper limit is set to keep enough difference of the air mass between the reference and observing-sky enough difference of the air mass between the ref erence and observing-sky.

3.2 Retrieval method

The vertical profiles of the ClO volume mixing ratio were retrieved by using the weighted-damped least squares fitting algorithm (Nagahama et al., 1999) based on the optimal estimation method (Rodgers, 1976). In the Rodgers's original method, the ClO volume mixing ratio $\mathbf{R}_{\mathrm{ret}}$ is estimated as

$$\mathbf{R}_{\mathrm{ret}} = \mathbf{R}_{\mathrm{a\,priori}} + \mathbf{S}_{\mathrm{R}}\mathbf{W}^{\mathrm{T}}\left(\mathbf{W}\mathbf{S}_{\mathrm{R}}\mathbf{W}^{\mathrm{T}} + \mathbf{S}_{\mathrm{sp}}\right)^{-1}(\mathbf{T}_B - \mathbf{W}\mathbf{R}_{\mathrm{a\,priori}}) \tag{10}$$

where $\mathbf{R}_{\mathrm{a\,priori}}$ is the a priori volume mixing ratio profile, $\mathbf{W}$ is the weighting function for the spectrum, $\mathbf{S}_{\mathrm{R}}$ and $\mathbf{S}_{\mathrm{sp}}$ are the covariances of the a priori mixing ratio profile and the measured spectrum, respectively. Nagahama et al. (1999) showed that we can put it $\mathbf{S}_{\mathrm{R}} = \zeta^2 U$, where $\mathbf{U}$ is the unit matrix and ξ is a proportional constant, since S_{R} is independent to the altitude. In addition, we can put $\mathbf{S}_{\mathrm{sp}} = \varepsilon^2\mathbf{U}$, where ϵ is a proportional constant, since the rms noise of the spectrum is expected to be the same over the observed frequency range and there is no significant channel-to-channel correlation in the spectrum (Nagahama et al., 1999). Then the Eq. (10) becomes

$$\mathbf{R}_{\mathrm{ret}} = \mathbf{R}_{\mathrm{a\,priori}} + \mathbf{W}^{\mathrm{T}}\left[\mathbf{W}\mathbf{W}^{\mathrm{T}} + (\varepsilon/\zeta)^2\right]^{-1}(\mathbf{T}_B - \mathbf{W}\mathbf{R}_{\mathrm{a\,priori}}) \tag{11}$$

where $(\varepsilon/\zeta)^2$ is an adjustable parameter, and it is empirically determined to improve the vertical resolution and to suppress the artificial oscillation of the retrieval solution. We set $(\varepsilon/\zeta)^2 = 0.16$ in this study.

The averaging kernel, $\mathbf{A}$, corresponding to the vertical resolution is given as

$$\mathbf{A} = \mathbf{W}^{\mathrm{T}}[\mathbf{W}\mathbf{W}^{\mathrm{T}} + (\varepsilon/\zeta)^2]^{-1}\mathbf{W} \tag{12}$$

AMTD
5, 1907–1945, 2012

By using this algorithm, the vertical resolution no longer depend on rms noise of each spectrum (Nagahama et al., 1999), and we can compare the diurnal variation with a fixed vertical resolution for all retrieved profiles. We applied the above algorithm to the central part of the averaged ClO spectra with a frequency range of 150 MHz. The averaged spectra were smoothed by taking 7 ch binding up and 5 ch moving average, and subtracted an artificial continuum baseline by fitting forth-polynomial for outside of the frequency range of the ClO emission. The temperature and the pressure vertical profiles are necessary for the retrieval calculation. The daily temperature and pressure data were obtained from NCEP reanalysis data (Lait et al., 2005) by using NASA Goddard Space Flight Center (GSFC) Automailer system, but the maximum altitude of the NCEP data is 49 km. Thus we extrapolated the vertical temperature and pressure profiles by using COSPAR International Reference Atmosphere (CIRA86) (Rees et al., 1990) above 49 km. As a priori profile, i.e. initial guess, of the ClO volume mixing ratio we used the average value of the daytime and the nighttime MIPAS model atmospheres (2001) in the mid-latitude region. The molecular l ine parameters were taken from Jet Propulsion Laboratory (JPL) Submillimeter, Millimeter, and Microwave Spectral Line Catalog (Pickett et al., 1992).

4 Results and discussion

4.1 Retrieved vertical profile

Figure 3 shows the typical averaged ClO spectrum. This spectrum was obtained in a local time range between 12:00–15:00. In Fig. 4, we show the vertical profile of ClO volume mixing ratio retrieved from the spectrum shown in Fig. 3. A priori profile for the retrieval is superposed as the dashed line in Fig. 4.

In order to evaluate the retrieval algorithm, we calculated the expected spectrum by using so-called forward model calculation. The forward model spectrum is integration of the derivative radiative transfer equation along the line of sight by assuming the

AMTD
5, 1907–1945, 2012

symmetrical Voigt line-profile function for the given vertical profile of molecular mixing ratio, temperature and pressure. The forward model spectrum is shown in Fig. 3 as the blue line. The difference between the observed spectrum and the forward model spectrum is shown in the lower panel of Fig. 3. We can evaluate the retrieval results by this residual value, and the rms of the residual is smaller than 1.8 mK for all retrieval results in this study.

In Fig. 5, we show the averaging kernel of the retrieval. The vertical resolution was defined as the full width at half maximum (FWFM) of the averaging kernel for each altitude. As we mentioned in the previous section, we used an adjustable parameter $(\varepsilon/\zeta)^2$ instead of the covariance of the vertical profile that is normally used in the optimal estimation method. Thus the vertical resolution is fixed and the averaging kernel is the same for all averaged spectra as discussed in Nagahama et al. (1999).

In the retrieval analysis, we focused the central 150 MHz frequency range to avoid the contamination of the baseline ripple, and the mixing ratio is not solved appropriately below 40 km. On the other hand, the vertical resolution is broad above 50 km as seen in Fig. 5 due to the limitation of the signal-to-noise of the spectra. Thus the most reliable values of the mixing ratio in this study are those from 40 to 50 km. Considering the peak altitude of the ClO mixing ratio in the mid-latitude region is around 40 km according to the previous studies (e.g. Ricaud et al., 1997; Nedoluha et al., 2011), the altitude range covers the main part of the ClO mixing ratio. We will focus the mixing ratio from 40 to 50 km in the discussion of diurnal variation. The vertical resolution are estimated to be ~12, ~17, and ~21 km at 35, 40, and 45 km altitudes, respectively.

4.2 Error analysis

In this sub-section, we will discuss the errors on the derived mixing ratio. Uncertainties of the input parameters in the retrieval process influence the precision of the results as random errors. Such uncertainties are (1) difference between the actual and assumed temperature vertical profiles, (2) difference in a priori profile of ClO, and (3) random noise on the spectral data. In addition, we will evaluate (4) the random error caused

AMTD
5, 1907–1945, 2012

in the measurement of atmospheric optical depth. Other systematic errors due to the observing system and the measurement procedure are discussed later by comparing with the previous observations with other instruments.

4.2.1 Difference in the temperature profiles

We used the vertical temperature profile derived from NCEP reanalysis data below 45 km and CIRA86 above 45 km as mentioned in the previous chapter. If the assumed temperature profile is different from the actual one, the difference causes an error in the forward model calculation in the retrieval process. We numerically evaluated the error due this effect as follows. First, we made a virtual temperature profile adding a constant offset to the original temperature profile. By using this virtual temperature profile, we ran the retrieval program and compared the both retrieval results derived from the original and the virtual temperature profiles. The typical amplitude of diurnal variation of the stratospheric temperature is estimated about 1 K at 40 km or 4 K at 60 km around a latitude of 20° S according to the previous study by Huang et al. (2010), and we applied a constant offset of 5 K to the original profile. In Fig. 6, we show the estimated error on the mixing ratio at each altitude. As a consequence, the error was estimated to be smaller than ∼1 % between 40 and 50 km, but the error abruptly increase up to ∼5 % below 35 km.

4.2.2 Error due to the a priori profile of ClO

In the inversion analysis like the optimal estimation method, the influence from a priori to the retrieval result is unavoidable. Since large diurnal variation of the ClO mixing ratio has been presented in the previous works (e.g. Solomon et al., 1984; Ricaud et al., 1997), and the influence due to a priori is particularly important issue. In this study, we used a single a priori profile for all the averaged spectra. The a priori is an average vertical profile of daytime and nighttime MIPAS Model Atmosphere in the mid-latitude region.

AMTD
5, 1907–1945, 2012

We estimated the typical error numerically in a manner similar to the case estimated for the difference of the temperature profile. We retrieved the mixing ratio for the daytime spectrum by using two different types of a priori, i.e. the daytime a priori and the day-and-night average a priori, respectively. Then we compared the retrieved profiles for the two types of the a priori. For the nighttime spectrum, we made the same comparison by using the nighttime a priori instead of the daytime one. Figure 7 shows the difference of retrieved profiles for the two different a priori, i.e. numerically estimated error. Although the absolute error amplitude for daytime spectrum and the nighttime spectrum are almost the same, the percentile error is larger for the nighttime spectrum, which reflects the smaller mixing ratio in the nighttime. Between 40 and 50 km, the error is smaller than ∼ +13 % for daytime spectra and ∼ −22 % for nighttime spectra.

4.2.3 Random noise on the spectrum

Next, we estimated the influence due to the noise that is generated mainly by the receiver system. First, we generated a virtual spectral data by adding random noise on a forward model spectrum that was calculated from a virtual but realistic vertical ClO profile. Then we applied the retrieval algorithm to the virtual spectrum and compared the retrieved vertical profile with the original input profile. Since the typical value of the rms noise of the averaged ClO spectra was 1.8 mK, we added random noise of 1.8 mK to the forward model spectrum. The difference between the retrieved profile and the input profile is shown in Fig. 8. The error due to random noise is minimum at 40 km, ∼11 %, and it increases to ∼21 % at 50 km.

4.2.4 Random error related with the atmospheric correction

We estimated the atmospheric optical depth by using the sky tipping method (Ulich et al., 1980). In this method, the effective sky temperature is assumed to be equal to the hot load temperature. Then the relationship between the output power for the hot-load and the observing-sky is expressed as

AMTD
5, 1907–1945, 2012

$$\Delta P = P_{\mathrm{hot}} - P_{\mathrm{sky}} \tag{13}$$

$$= \alpha\left\{T_{\mathrm{hot}} - T_{\mathrm{trop}}\left[1 - \exp\left(-\frac{\tau}{\sin \mathrm{El}}\right)\right]\right\} \tag{14}$$

$$= \alpha T_{\mathrm{hot}} \exp\left(-\frac{\tau}{\sin \mathrm{El}}\right) \quad (\because \quad T_{\mathrm{hot}} = T_{\mathrm{trop}}) \tag{15}$$

The temperature of the hot load is stable and equal to the room temperature, 300 K which is controlled by an air conditioner. Then, the logarithm of the difference of the output power, $\ln(\Delta P)$, becomes a function of sky optical depth τ and the air mass factor, and the relationship is written as $A_{\mathrm{El}}\left(\equiv \frac{1}{\sin \mathrm{El}}\right)$,

$$\ln(\Delta P) = -\tau A_{\mathrm{El}} + \ln(\alpha T_{\mathrm{hot}}) \,. \tag{16}$$

In this relationship, the τ is a proportional constant. We can determine the τ by measuring the values of ΔP for several elevation angles. This is the sky tipping method.

However, the actual sky temperature changes from hour to hour, and the difference between the actual effective sky temperature and the hot-load temperature causes the error of the sky optical depth τ. The effective sky temperature is typically by ~7 K smaller than the surface temperature (Parrish et al., 1988). In the observing period in December 2009, the outside surface temperature was around 300 K in day and around 275 K in the night at Atacama. Considering such an outside temperature fluctuations, the optical depth τ varies ~12 % at most if we change the sky effective temperature between 270 K and 300 K. In addition, the error of τ_{plate} is almost the same because we estimated τ_{plate} from the sky optical depth by using the Eq. (9). We have numerically estimated the influence of these optical depths and the sky temperature errors on the retrieval calculation of the mixing ratio. The results are shown in Fig. 9. The error on the mixing ratio is estimated within 2–7 % from 40 to 50 km.

AMTD
5, 1907–1945, 2012

4.2.5 Total of the random errors

We evaluated the random errors caused by four sources. The total of the random errors can be expressed by root sum square of each error since the four types of errors that we evaluated above are considered to be independent one another. The total random error is shown in Fig. 10. Among the four causes, the contributions of the a priori and the noise of the spectral data are similar level and account for the major portion of to the total error.

4.2.6 Systematic errors

Systematic errors influence the accuracy of the results. They are mainly caused by some biases related with the characteristics of the observation system or the calibration methods of the signal intensity. In our measurement system in Atacama, we used two blackbodies at different physical temperatures as the references of intensity. The cold load is a radio absorber soaked in liquid nitrogen, and the cold-load temperature is expected to be very stable. But the cooled radio absorber is seen through the vessel made by styrene foam, and the opacity of the styrene foam effectively increases the brightness temperature of the cold load by less than ∼3 %. On the other hand, the hot load is in equilibrium with the room temperature. The room temperature roughly changes within ±5 K between day and night, so the intensity scale of the spectra varies at most ∼ ±2 % between day and night.

Other systematic error related intensity calibration is due to the imbalance of the sideband ratio of the heterodyne mixer receiver. We used a superconductive double sideband mixer that is sensitive both upper and lower input frequency band, and we assume that the gains of the upper and lower sidebands are equal. The calibration signals from the hot- and cold-loads come in the both sidebands, while the spectral signal comes from only one sideband. If the actual gains of the two sidebands are not equal, it causes a systematic error in the intensity scale. However, it is practically difficult to measure the side band ratio precisely for a double side band superconductive mixer,

AMTD
5, 1907–1945, 2012

and final evaluation of the accuracy of the intensity calibration is made by comparisons with data obtained by other instruments.

4.3 Comparison with the satellite measurements

To evaluate the total systematic error, we will compare the retrieval results for Atacama with other satellite measurements. First, we use AURA/MLS v2.2 data for this purpose. We selected the ClO profiles from AURA/MLS database by criteria of the positional coincidence within ±2° in latitude and ±30° N longitude from the position of the Atacama station and the time coincidence in 12:00–15:00 LT between 5 and 16 December 2011. Finally, 35 profiles were selected. We averaged them and convolved by the Atacama averaging kernel in order to equalize the vertical resolution and response, because the vertical resolution of AURA/MLS is higher than that of Atacama retrieval. The convolved and the original profiles of MLS and Atacama retrieved profile are shown in Fig. 11. The error bar for the MLS mixing ratio in Fig. 11 is derived from the precision value attached to the individual profiles. In the original MLS profile, the mixing ratio at 50 km looks unrealistically large, since the mixing ratio peak appears around 35–40 km in the previous studies such as Nedoluha et al. (2011) over Mauna Kea and other ground-based data in Ricaud et al. (1997) over Plateau de Bure. In addition, Santee et al. (2008) mentioned that the MLS mixing ratio below 1.0 hPa corresponding above ~50 km is unsuitable for scientific use. On the other hand, Atacama profile is not reliable below 40 km as we mentioned in the Sect. 4.1. Thus, we can make fruitful comparison only at 40 and 45 km.

The mixing ratios of Atacama measurements show slightly positive biases to those of MLS, which are ~13 % and ~18 % at 40 and 45 km, respectively, but both measurements agree with each other within the errors. The mixing ratio at 40 km in other previous studies in Nedoluha et al. (2011) and Ricaud et al. (1997) are ~0.5 ppbv. Thus the positive bias to the MLS mixing ratio is likely, although we cannot directly compare them because of the difference of the observing site location and observing time.

AMTD
5, 1907–1945, 2012

Next, we will compare with the JEM/SMILES data. SMILES has three observing frequency bands, but two of the three frequency bands can be operated simultaneously. Unfortunately, SMILES did not observe band C which covers the ClO line frequency during the observational period in Atacama. Therefore, it is difficult to directly compare with the SMILES data, we can roughly evaluate the Atacama results by using the SMILES data obtained November 2009 and January 2010.

Figure 12 shows the time series of the ClO mixing ratio at 40 and 50 km obtained by SMILES. The plotted data are selected from the version 1.3 (test release) dataset by applying the same positional criteria used for AURA/MLS. On Fig. 12, we plotted the mixing ratio of Atacama measurements as well. The mixing ratio of Atacama measurements at 40 km looks reasonable, roughly on the line linearly interpolated the values in November and January of the SMILES mixing ratio. At 50 km, the mixing ratio of SMILES is slightly decreasing but can be regarded almost constant compared with that at 40 km. Atacama mixing ratio at 50 km looks larger by about 80 % than the average value of the SMILES, but the large discrepancy is interpreted in terms of the averaging kernel of Atacama measurements. If we make convolution of the SMILES profile with the Atacama averaging kernel at 50 km, the discrepancy is reduced to ∼7 %. Therefore, it is likely that Atacama ground-based meas urements are consistent with the SMILES measurements within the error, although the exact coincident datasets for the direct comparison do not exist.

4.4 Diurnal variation of stratospheric ClO observed over Atacama

Photochemistry of the chlorine reservoir species such as $ClONO_2$, HOCl, and HCl play an important role to regulate the diurnal variation of ClO (e.g. Ko and Sze, 1984; Froidevaux et al., 1985). Among the reservoir species, HCl is the most abundant one, but its chemical life time is long enough, more than 1 day (Brasseur and Solomon, 1984). Thus, $ClONO_2$ and HOCl are considered to make a major contribution to the diurnal variation of ClO.

AMTD
5, 1907–1945, 2012

Observationally, the first full-time frame, i.e. over 24 h diurnal variation of stratospheric ClO was presented by Solomon et al. (1984). They revealed the variation of total intensity of ClO spectra that were obtained at every two hours in October and December, 1982 over Mauna Kea, Hawaii (19.5° N). The total intensity traces the column density of ClO above 30 km. They found significant increase and decrease after the sunrise and the sunset, respectively, but the observed increasing rate was slower than that expected from the model predictions (Ko and Sze, 1984). The next dataset concerning the diurnal variation was presented by Ricaud et al. (1997). They studied the altitudinal dependence of the ClO diurnal variation based on the retrieved vertical profiles derived every hour from the ground-based millimeter-wave spectroscopy in 3–5 January 1995 over Plateau de Bure, France (45° N). The time variation curve has shown good agreement with the model calculations within 0.1 ppbv. They mentioned that the mixing ratio at one hour after noon was upshifted at all height between 25 and 50 km, although such an abrupt increase has not been predicted by model calculations. After that, Ricaud et al. (2000) used the satellite data obtained by UARS/MLS from 1991 to 1997 to improve the signal-to-noise ratio. They selected and averaged the ClO data within a latitude band from 40 to 50° N irrespective of the year, and they also calculated photochemical time evolution based on the observed data of various related molecules such as O_3, HCl, $ClONO_2$, NO_2, H_2O, and CH_4 by using the instruments aboard the UARS satellite. The MLS data over the 7 yr provided firmer values of the ClO mixing ratio with small scatter and errors, and the observed diurnal variations have shown good agreement with their photochemical calculations. They revealed that the partitioning within the ClO_x (= Cl + ClO) that is proportional to O/O_3 plays a major role in the diurnal variation above 50 km rather than the photochemistry of $ClONO_2$ and HOCl.

The present study shows the ClO diurnal variation in the Southern Hemisphere obtained by the ground-based millimeter-wave measurements over Atacama, Chile. Figure 13 shows the diurnal variation of ClO at 40, 45 and 50 km, averaged over 5–16 December 2009 over Atacama (23° S). The horizontal axis is the local time, LT, in Chile.

AMTD
5, 1907–1945, 2012

The vertical profiles are derived from the averaged spectra for every 3-h bin from 00:00 to 24:00 over the 12 days. During this period, the sunrise time and the sunset time were 05:30 and 19:30, respectively, and the culmination time was 12:30 at Aacama. At 40 km, the mixing ratio of ClO quickly increases after the sunrise and reaches up to the daytime plateau level at the time slot of 06–09 LT, while the increasing rate at 45 km is slower than that at 40 km, taking more than 3 h to increase up to the daytime plateau level. On the other hand, the mixing ratio at the time slot of 18–21 LT corresponding to the sunset still keeps the daytime plateau level, suggesting that the day time mixing ratio persists for about two hours after the sunset (19:30) both at 40 km and 45 km. After 21:00, the mixing ratio of ClO decreases monotonically throughout the nighttime before the sunrise. During the day time from 9 to 21 LT, the daytime plateau level is almost constant at all altitudes between 40 and 50 km. There is no significant increase after noon that mentioned in Ricaud et al. (2000), but it is not conclusive taking the error and the coarse time resolution of the present measurement. The amplitude of the diurnal variation of ClO is 0.17, 0.17 and 0.14 ppbv at 40, 45 and 50 km, respectively.

In Fig. 14, we show the summer time diurnal variation of ClO presented in Ricaud et al. (2000) superposing on the variation curve of Atacama measurements. For comparison, we have we have convolved the Ricauds's data by the Atacama averaging kernel of in order to equalize the vertical resolution and averaged over every 3 h. The reference level in the vertical axis is normalized to the average value over 24 h for both datasets. The horizontal axis for the Ricauds's data is local solar time, while that for Atacama data is local time in Chile. There is about 30 min difference between them based on the culmination time. The sunrise time for the Ricauds's data, i.e. at 45° N in July, is ~04:30 that is one hour prior to Atacama, and the sunset time is ~19:30 that is almost same as Atacama. The nominal altitude of the three panels in Fig. 14 are 40, 45, and 50 km for Atacama measurements and the corresponding altitudes for the Ricauds's measurements are 41, 47, and 53 km, respectively.

At 40 km, the amplitude of the diurnal variation is almost the same between the two measurements. At 45 and 50 km, the amplitudes are almost the same within the

AMTD
5, 1907–1945, 2012

error, but there is a tendency that the daytime plateau level is slightly larger in the present measurements in Atacama. In addition, a slight increase around the sunset time can be seen in the Ricauds's measurement, but there is no significant feature over Atacama. The slight upshift around the sunset above 45 km is due to the change of ClO_x partitioning that related with the fast catalytic depletion cycle of ozone. This ClO_x partitioning does not influence significantly at 40 km or lower. Another difference between the two measurements is seen in the increasing rate around the sunrise. The increasing rate becomes slower with altitude in the Atacama data. Although the sunrise time is one hour delayed in the Ricauds's measurements, the difference of increasing rates is significant even if we consider the delay of the sunrise time of the Ricauds' data. It may be related with the difference of solar irradiance between Atacama (23° S) and Plateau de Bure (45° N). The shape of the averaging kernel may influence as well. For further discussion, it is necessary to run a model calculation that is fitted for the Atacama site to compare with the observational results. We intend to make such a comparison with model calculation in the next paper.

5 Summary

This paper has presented the vertical profiles and the diurnal variation of ClO in the summer time in the southern mid-latitude region, based on the new millimeter-wave spectroscopic measurements made in the Atacama highland, Chile. We have described the specification of the new measurement system, the observing method, and the retrieval method of vertical mixing ratio profiles. The measurement errors have been evaluated numerically, and the precision of the ClO mixing ratio is estimated from 20 to 30 % in an altitude range from 40 to 50 km. We have presented the diurnal variation of the ClO over 24 h from 40 to 50 km during 5–16 December, 2009. The variation amplitude and variation pattern at 40 km is consistent with the previous study in the northern mid-latitude presented by Ricaud et al. (2000). At 45 and 50 km, the amplitudes are slightly larger than those of Ricaud et al. (2000), and the increasing rates

AMTD
5, 1907–1945, 2012

after the sunrise are smaller than those of Ricaud et al. (2000). We intend to continue further observations to reveal the seasonal variations as well as the diurnal variation and intend to make model calculation to compare the observational results.

Acknowledgements. JEM/SMILES mission is a joint project of Japan Aerospace Exploration Agency (JAXA) and National Institute of Information and Communications Technology (NICT).

References

Amano, T., Hirota, E., and Morino, Y.: Microwave spectrum of the ClO radical, J. Molec. Spectrosc., 27, 257–265, 1968. 1910

Brasseur, G. and Solomon, S.: Composition and chemistry, in: Aeronomy of the Middle Atmosphere, Chapt. 5, D. Reidel Publishing Co, Dordrecht, 440 pp, 1984. 1924

De Zafra, R. L., Emmons, L. K., Reeves, J. M., and Shindell, D. T.: An overview of millimeter-wave spectroscopic measurements of chlorine monoxide at Thule, Greenland, February–March, 1992: Vertical profiles, diurnal variation, and longer-term trends, Geophys. Res. Lett., 21, 1271–1274, doi:10.1029/93GL01677, 1994. 1909

Emmons, L. K., Shindell, D. T., Reeves, J. M., and de Zafra, R. L.: Stratospheric ClO profiles from McMurdo Station, Antarctica, spring 1992, J. Geophys. Res., 100, 3049–3056, doi:10.1029/94JD02962, 1995. 1909

Froidevaux, L., Allen, M., and Yung, Y. L.: A critical analysis of ClO and O_3 in the mid-latitude stratosphere, J. Geophys. Res., 90, 12999–13029, doi:10.1029/JD090iD07p12999, 1985. 1924

Huang, F. T., McPeters, R. D., Bhartia, P. K., Mayr, H. G., Frith, S. M., Russell III, J. M., and Mlynczak, M. G.: Temperature diurnal variations (migrating tides) in the stratosphere and lower mesosphere based on measurements from SABER on TIMED, J. Geophys. Res., 115, D16121, doi:10.1029/2009JD013698, 2010. 1919

Jones, A., Urban, J., Murtagh, D. P., Sanchez, C., Walker, K. A., Livesey, N. J., Froidevaux, L., and Santee, M. L.: Analysis of HCl and ClO time series in the upper stratosphere using satellite data sets, Atmos. Chem. Phys., 11, 5321–5333, doi:10.5194/acp-11-5321-2011, 2011.

Kuwahara, T., Mizuno, A., Nagahama, T., Maezawa, H., Morihira, A., Toriyama, N., Murayama, S., Matsuura, M., Sugimoto, T., Asayama, S., Mizuno, N., Onishi, T., and Fukui, Y.:

AMTD

5, 1907–1945, 2012

Ground-based millimeter-wave observations of water vapor emission (183 GHz) at Atacama, Chile, Adv. Space Res., 42, 1167–1171, doi:10.1016/j.asr.2007.11.030, 2008. 1910
Lait, L., Newman, P., and Schoeberl. R.: The Goddard Automailer, available online at: http://code916.gsfc.nasa.gov/Data_services/ (last access: 5 February 2010), 2005. 1917
Mahieu, E., Zander, R., Duchatelet, P., Hannigan, J. W., Coffey, M. T., Mikuteit, S., Hase, F., Blumenstock, T., Wiacek, A., Strong, K., Taylor, J. R., Mittermeier, R., Fast, H., Boone, C. D., McLeod, S. D., Walker, K. A., Bernath, P. F., and Rinsland, C. P.: Comparisons between ACE-FTS and groundbased measurements of stratospheric HCl and $ClONO_2$ loadings at northern latitudes, Geophys. Res. Lett., 32, L15S08, doi:10.1029/2005GL022396, 2005. 1909
Malcom K. W. and Sze, N. D.: Diurnal variation of ClO: Implications for the stratospheric Chemistries of $ClONO_2$, HOCl, and HCl, J. Geophys. Res., 89, 11619–11632, doi:10.1029/JD089iD07p11619, 1984. 1924, 1925
Mizuno, A., Nagahama, T., Morihira, A., Ogawa, H., Mizuno, N., Yonekura, Y., Yamamoto, H., Nakane, H., and Fukui, Y.: Millimeterwave radiometer for the measurement of stratospheric ClO using a superconductive (SIS) receiver installed in the Southern hemisohere, Int. J. Infrared Milli., 23, 981–995, doi:10.1023/A:1019618917005, 2002. 1910, 1911, 1912
Molina, M. and Rowland, F. S.: Stratospheric sink for chlorofluoromethanes: chlorine atomic catalysed destruction of ozone, Nature, 249, 810–814, doi:10.1038/249810a0, 1974. 1908
Nagahama, T., Nakane, H., Fujinuma, Y., Ninomiya, M., Ogawa, H., and Fukui, Y.: Ground-based millimeter-wave observations of ozone in the upper stratosphere and mesosphere over Tsukuba, Earth Planet. Space, 51, 1287–1296, 1999. 1916, 1917, 1918
Nedoluha, G. E., Connor, B. J., Barrett, J., Mooney, T., Parrish, A., Boyd, I., Wrotny, J. E., Gomez, R. M., Koda, J., Santee, M. L., and Froidevaux, L.: Ground-based measurements of ClO from Mauna Kea and intercomparisons with Aura and UARS MLS, J. Geophys. Res., 116, D02307, doi:10.1029/2010JD014732, 2011. 1909, 1918, 1923
Parrish, A., de Zafra, R. L., Solomon, P. M., and Barrett, J. W.: A ground-based technique for millimeter wave spectroscopic observations of stratospheric trace constituents, Radio Sci., 23, 106–118, 1988. 1921
Pickett, H. M., Poynter, R. L., and Cohen, E. A.: Submillimeter, millimeter and microwave spectral line catalog, Tech. Rep., 80–23, Rev. 3, Jet Propulsion Lab., Pasadena, CA, 217 pp., 1992. 1917
Raffalski, U., Klein, U., Franke, B., Langer, J., Sinnhuber, B.-M., Trentmann, J., Künzi, K. F., and Schrems, O.: Ground based millimeter-wave observations of Arctic chlorine activation during

AMTD
5, 1907–1945, 2012

winter and spring 1996/97, Geophys. Res. Lett., 25, 3331–3334, doi:10.1029/98GL52487, 1998. 1909

Rees, D., Barnett, J. J., and Labitzke, K.: COSPAR International Reference Atmosphere: 1986, Part II: Middle atmosphere models, Pergamon Press, Oxford, UK, 1990. 1917

Ricaud, P., de La Noë, J., Lauqué, R., and Parrish, A.: Analysis of stratospheric chlorine monoxide measurements recorded by a ground-based radiometer located at the Plateau de Bure, France, J. Geophys. Res., 102, 1423–1439, doi:10.1029/96JD01724, 1997. 1918, 1919, 1923, 1925

Ricaud, P., Chipperfield, M. P., Waters, J. W., Russell III, J. M., and Roche, A. E.: Temporal evolution of chlorine monoxide in the middle stratosphere, J. Geophys. Res., 105, 4459–4469, doi:10.1029/1999JD900995, 2000. 1909, 1925, 1926, 1927, 1928, 1945

Rinsland, C. P., Mahieu, E., Zander, R., Jones, N. B., Chipperfield, M. P., Goldman, A., Anderson, J., Russell III, J. M., Demoulin, P., Notholt, J., Toon, G. C., Blavier, J.-F., Sen, B., Sussmann, R., Wood, A., Meier, D. W. T., Griffith, L. S., Chiou, F. J., Murcray, T. M., Stephen, F., Hase, S., Mikuteit, A., Schulz, S. W., and Blumenstock, T.: Long-term trends in inorganic chlorine from ground based infrared solar spectra: past increases and evidence for stabilization, J. Geophys. Res., 108, 4252, doi:10.1029/2002JD003001, 2003. 1909

Rodgers, C. D.: Retrieval of atmospheric temperature and composition from remote sounding measurements of thermal radiation, Rev. Geophys., 14, 609–624, doi:10.1029/RG014i004p00609, 1976. 1916

Santee, M. L., Lambert, A., Read, W. G., Livesey, N. J., Manney, G. L., Cofield, R. E., Cuddy, D. T., Daffer, W. H., Drouin, B. J., Froidevaux, L., Fuller, R. A., Jarnot, R. F., Knosp, B. W., Perun, V. S., Snyder, W. V., Stek, P. C., Thurstans, R. P., Wagner, P. A., Waters, J. W., Connor, B., Urban, J., Murtagh, D., Ricaud, P., Barrett, D., Kleinboehl, A., Kuttippurath, J., Kullmann, H., von Hobe, M., Toon, G. C., and Stachnik, R. A.: Validation of the Aura Microwave Limb Sounder ClO measurements, J. Geophys. Res., 113, D15S22, doi:10.1029/2007JD008762, 2008. 1923

Solomon, P. M., de Zafra, R., Parrish, A., and Barrett, J. W.: Diurnal variation of stratospheric chlorine monoxide: a critical test of chlorine chemistry in the ozone layer, Science, 224, 1210–1214, doi:10.1126/science.224.4654.1210, 1984. 1909, 1919, 1925

Solomon, P. M., Barrett, J., Mooney, T., Connor, B., Parrish, A., and Siskind, D. E.: Rise and decline of active chlorine in the stratosphere, Geophys. Res. Lett., 33, L18807, doi:10.1029/2006GL027029, 2006.

AMTD
5, 1907–1945, 2012

Tucker, J. R. and Feldman, M. J.: Quantum detection at millimeter wavelength, Rev. Mod. Phys., 57, 1055–1113, 1985. 1911

Ulich, B. L., Davis, J. H., Rhodes, P. J., and Hollis, J.: Absolute brightness temperature measurements at 3.5-mm wavelength, IEEE T. Antenn. Propag., 28, 367–376, doi:10.1109/TAP.1980.1142330, 1980. 1914, 1920

World Meteorological Organization (WMO): Sientific Assesment of Ozone Depletion, 2010, Genova, 2011. 1909

Zander, R., Mahieu, E., Gunson, M. R., Abrams, M. C., Chang, A. Y., Abbas, M., Aellig, C., Engel, A., Goldman, A., Irion, F. W., Kämpfer, N., Michelson, H. A., Newchurch, M. J., Rinsland, C. P., Salawitch, R. J., Stiller G. P., and Toon, G. C.: The 1994 northern mid-latitude budget of stratospheric chlorine derived from ATMOS/ATLAS 3 observations, Geophys. Res. Lett., 23, 2357–2360, doi:10.1029/96GL01792, 1996. 1908

AMTD

5, 1907–1945, 2012

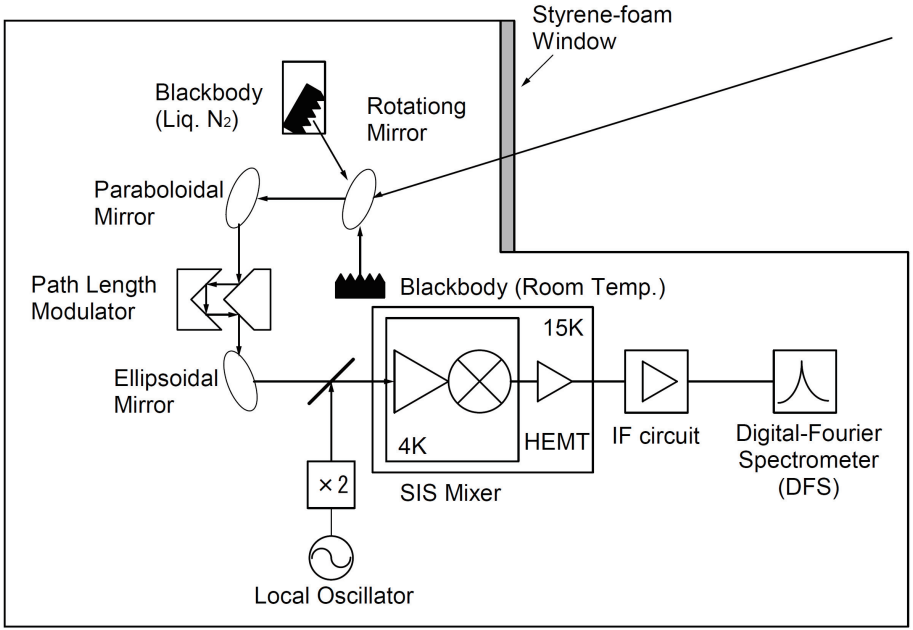

Fig. 1. The block diagram of the millimeter-wave spectroscopic radiometer in Atacama, Chile.

AMTD
5, 1907–1945, 2012

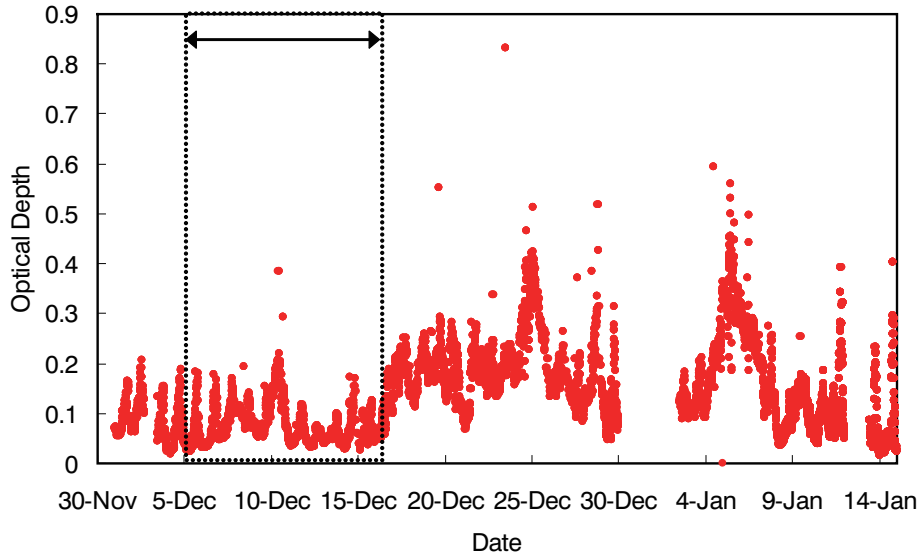

Fig. 2. Time series of optical depth from 1 December 2009 to 17 January 2010. The left-right arrow shows the period of analysis data from 5 to 16 December 2009.

AMTD
5, 1907–1945, 2012

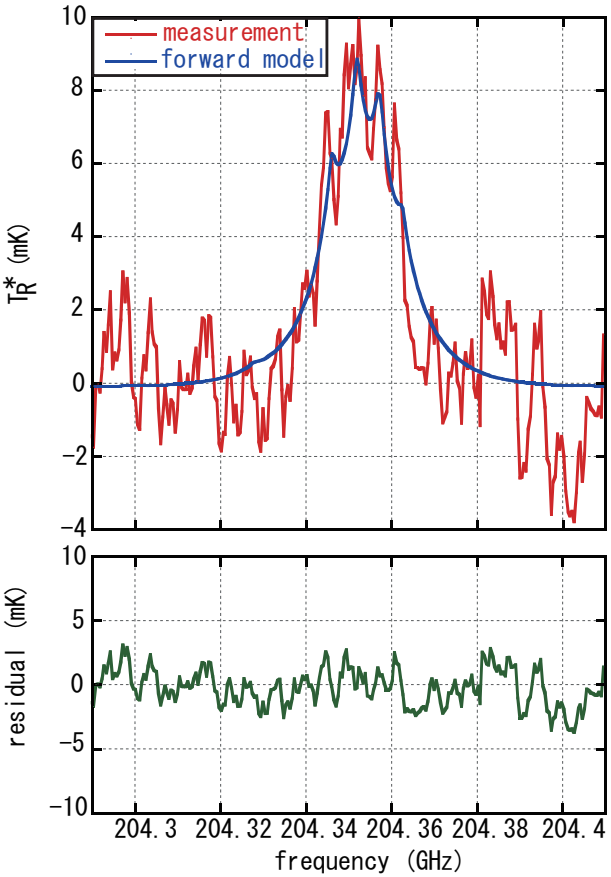

Fig. 3. Upper panel: Close up view at the center of the ClO spectrum observed at 12:00–15:00 LT from 5 to 16 December 2009. A red line shows the ClO spectrum with the Atacama radiometer. A blue line shows fitting curve with forward model. Lower panel: The residual of fitting by the forward model calculation.

AMTD
5, 1907–1945, 2012

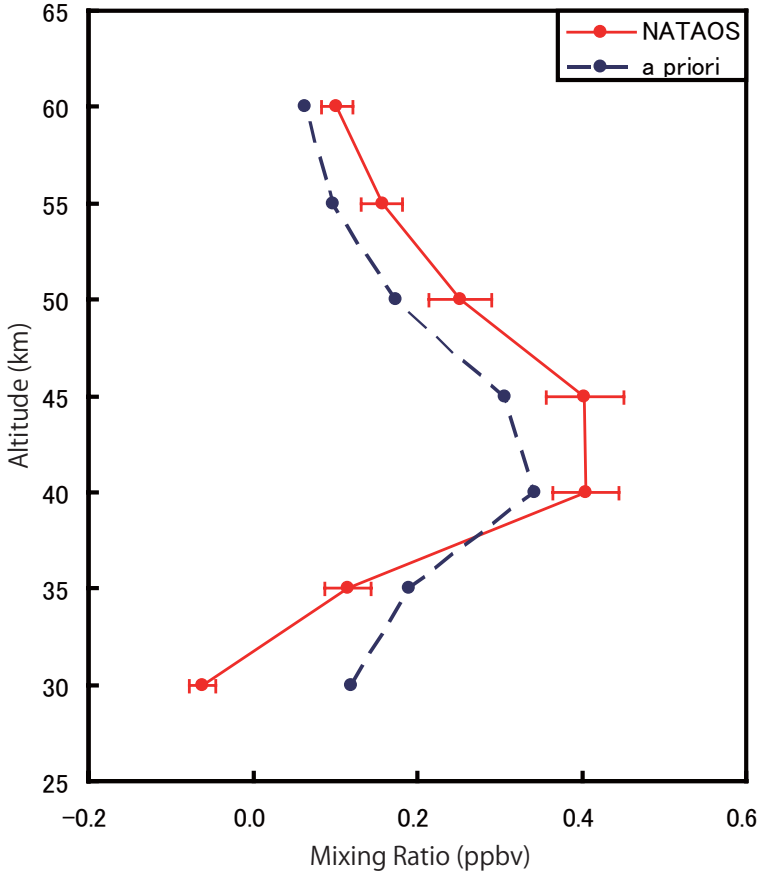

Fig. 4. The retrieved vertical profile of ClO mixing ratio (red line) with the a priori profile (blue line). The retrieved vertical profile was observed 12:00–15:00 LT from 5 to 16 December 2009.

AMTD
5, 1907–1945, 2012

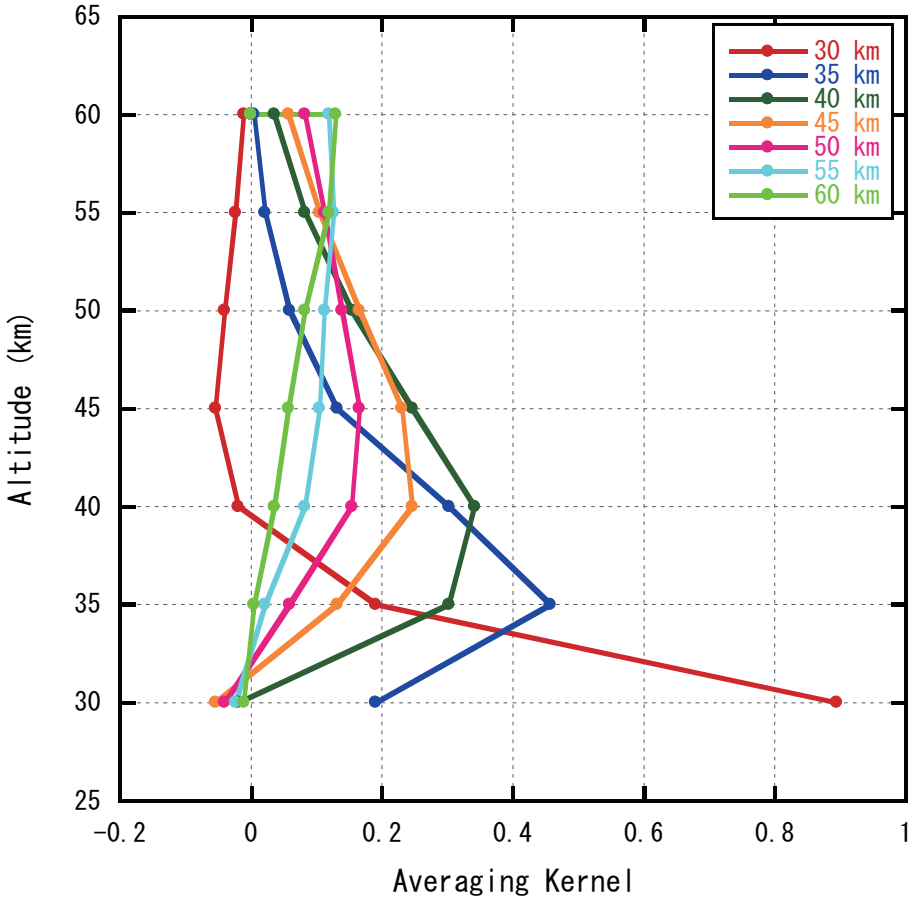

Fig. 5. The averaging kernel for retrieval calculation between 30 and 60 km by 5 km steps.

AMTD
5, 1907–1945, 2012

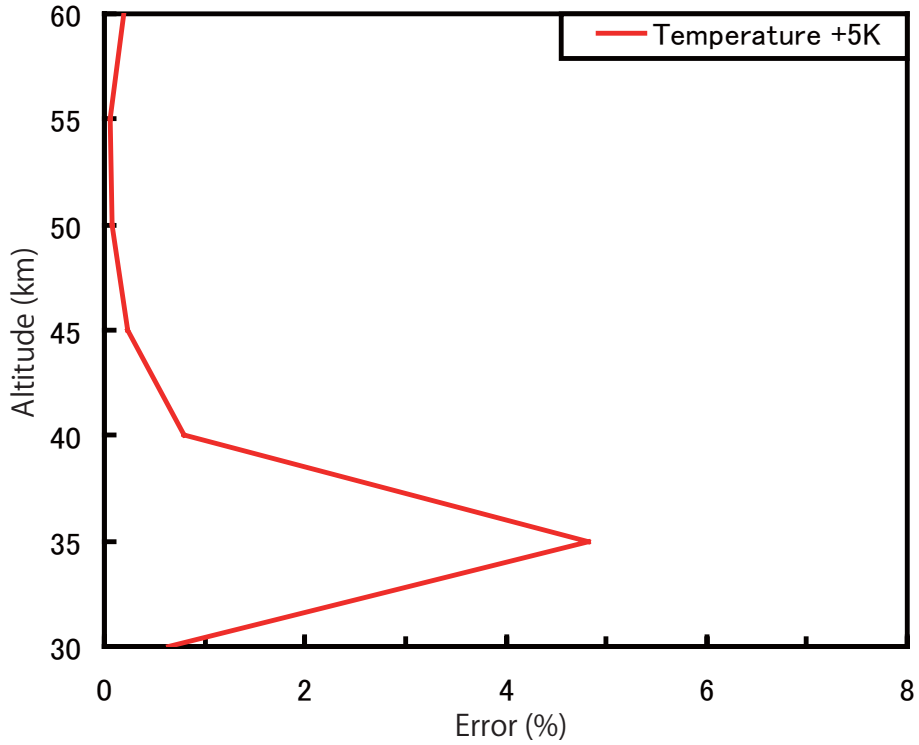

Fig. 6. Estimated random errors on the retrieval due to the temperature difference.

AMTD
5, 1907–1945, 2012

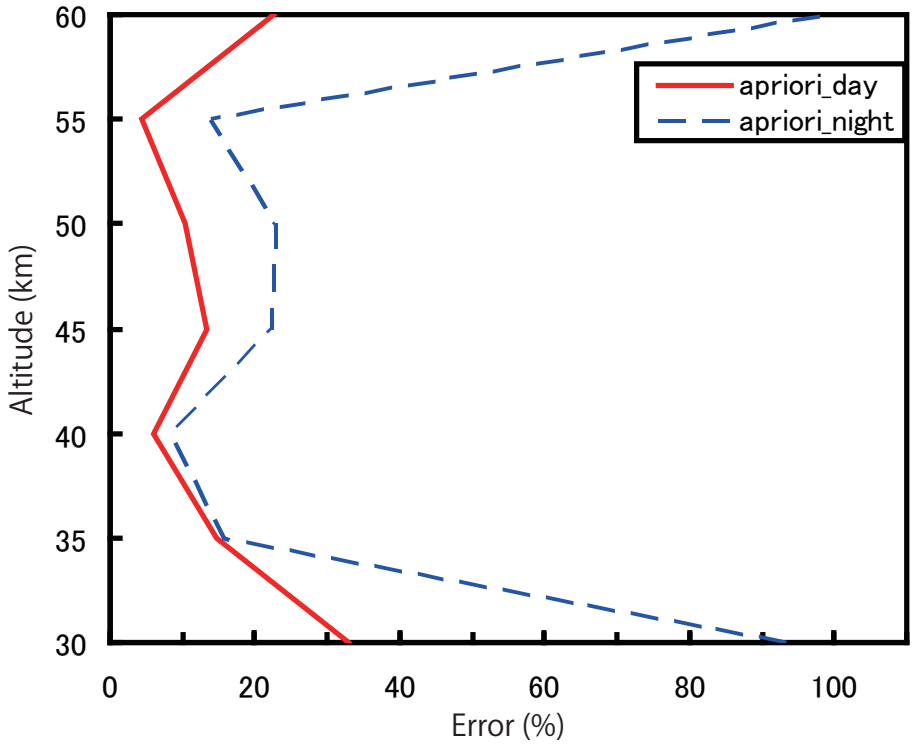

Fig. 7. Estimated random error on the retrieval due to errors in the a priori profiles of ClO. The red line are the case that the error is estimated for daytime spectrrum. The bule line are the case that the error is estimated for nighttime spectrum.

AMTD
5, 1907–1945, 2012

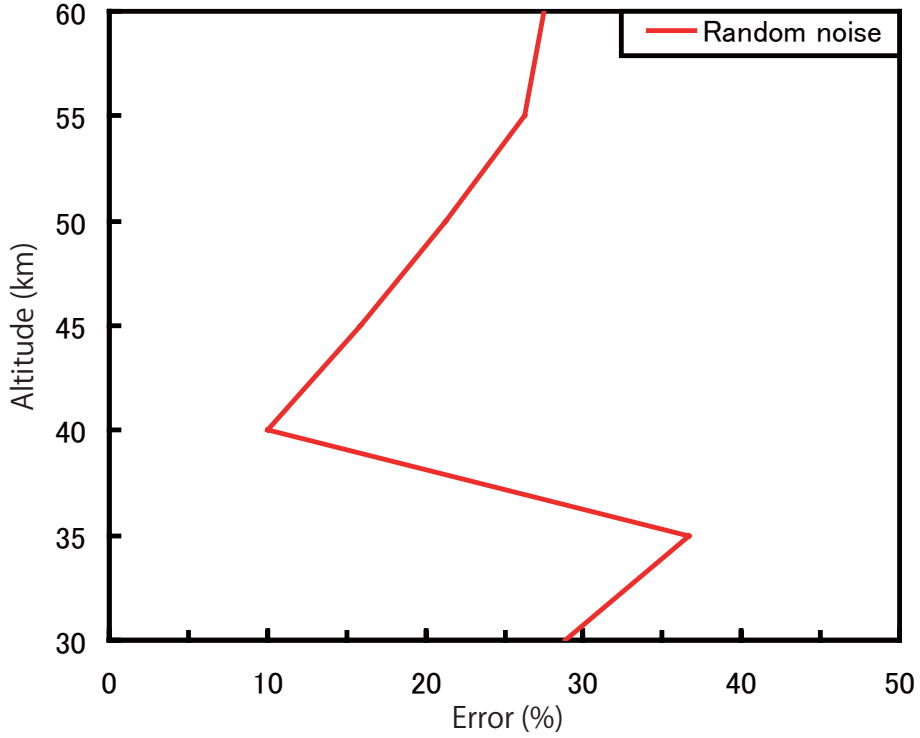

Fig. 8. Estimated random error on the retrieval due to random noise on the spectra.

AMTD
5, 1907–1945, 2012

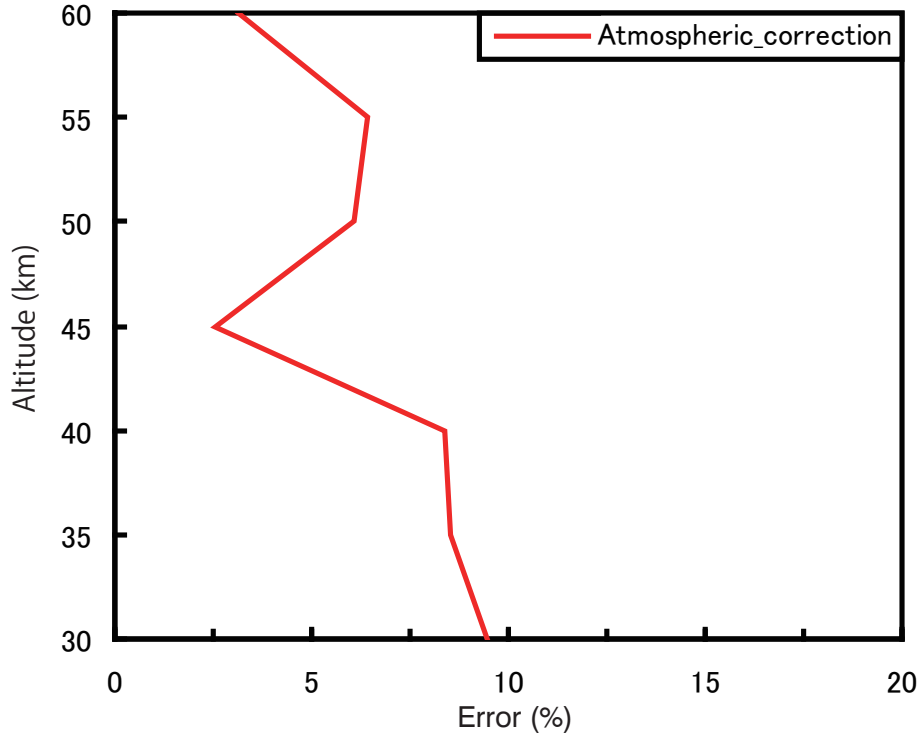

Fig. 9. Estimated random error related with the atmospheric correction.

AMTD
5, 1907–1945, 2012

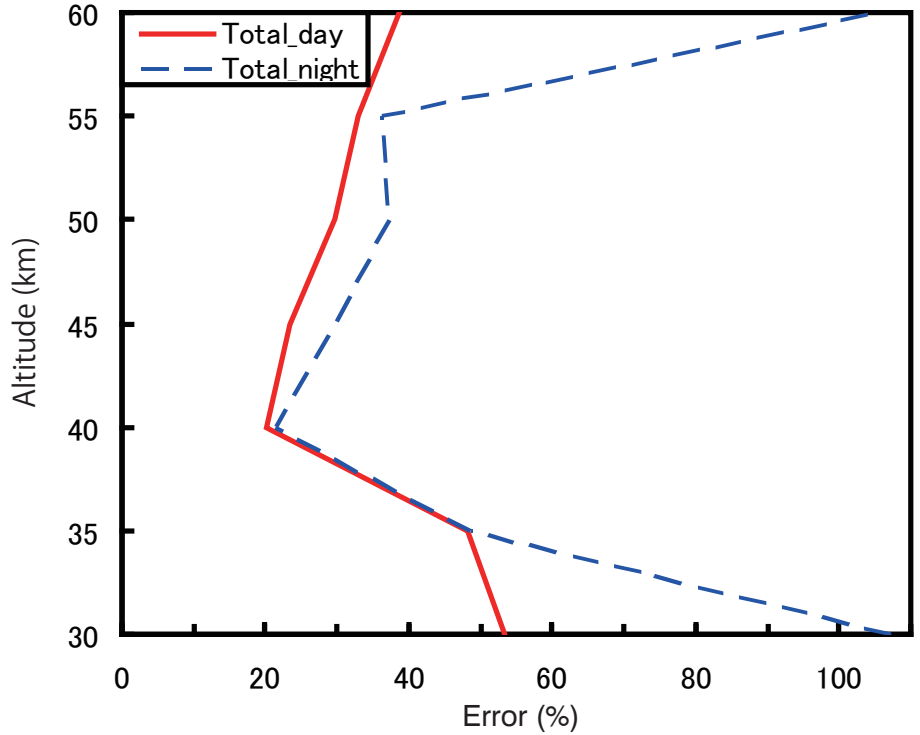

Fig. 10. Total of the random errors on the retrieval.

AMTD
5, 1907–1945, 2012

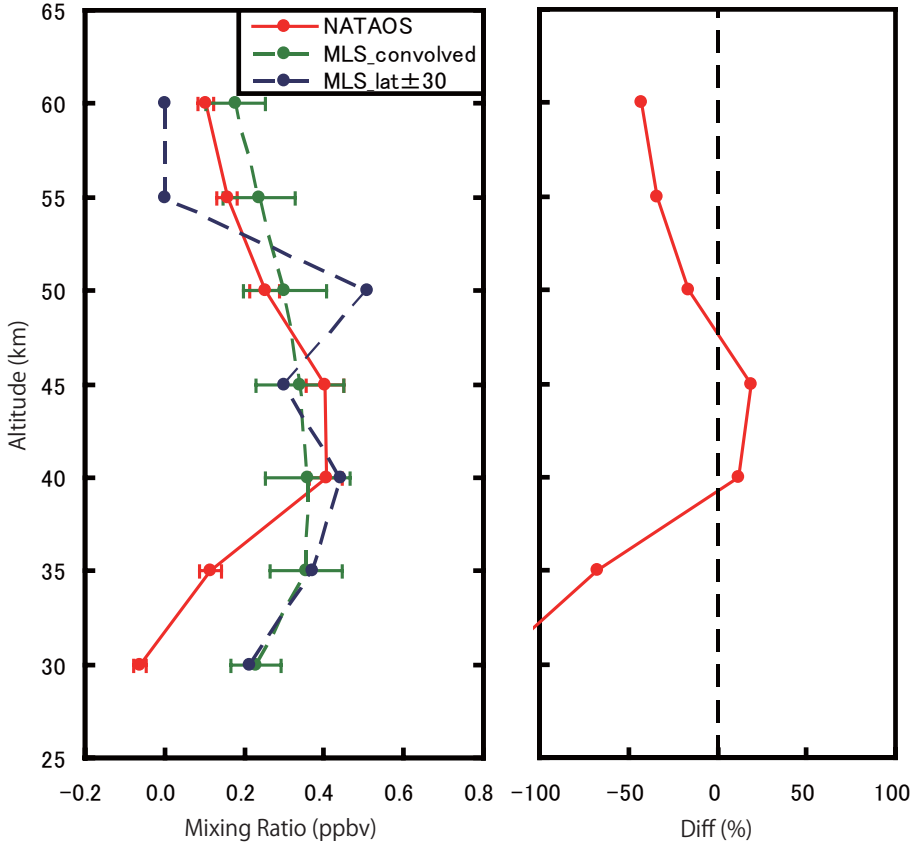

Fig. 11. Comparison of the vertical profile measured by Atacama radiometer and AURA/MLS. (Left) The red line shows the vertical profile of ClO measured by Atacama radiometer. The Aura/MLS v2.2 data within the area over Atacama (longitude: ±30°, latitude ±2°) is shown both for unconvolved (blue) and convolved (green) data. (Right) The percentage difference between Atacama radiometer and convolved AURA/MLS data.

AMTD
5, 1907–1945, 2012

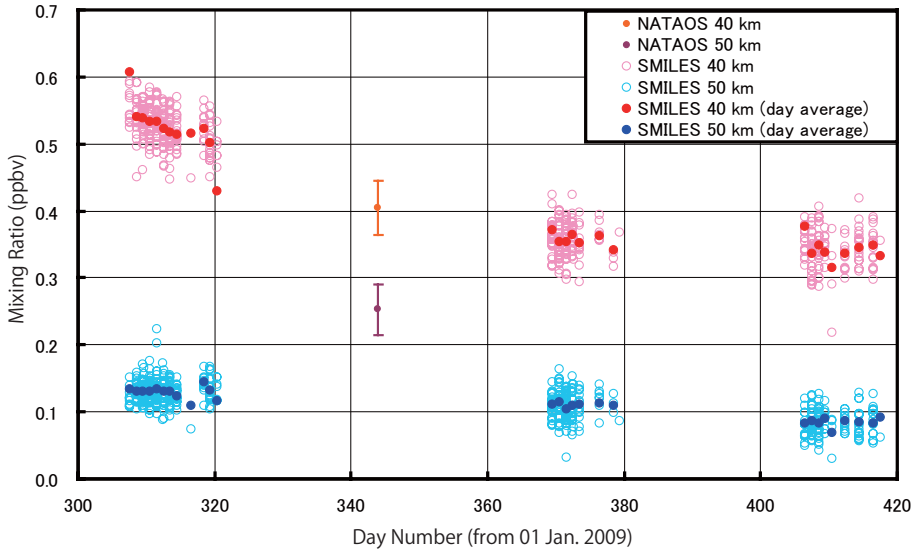

Fig. 12. The ClO mixing ratio at 40 and 50 km were obtained by JEM/SMILES and Atacama radiometer from November 2009 to February 2011. The ClO mixing ratio from JEM/SMILES v1.3 data within ±2° in latitude and ±30° in longitude and with an observational time of 12:00–15:00 LT. The pink and light blue open circle show the ClO mixing ratio obtained JEM/SMILES at 40 and 50 km, respectively. The red and blue circles show the day average of ClO mixing ratio obtained JEM/SMILES at 40 and 50 km, respectively. The orange and purple circles show the ClO mixing ratio obtained by Atacama radiometer at 40 and 50 km, respectively. The light-left arrow shows the period of analysis data from 5 to 16 December 2009.

AMTD
5, 1907–1945, 2012

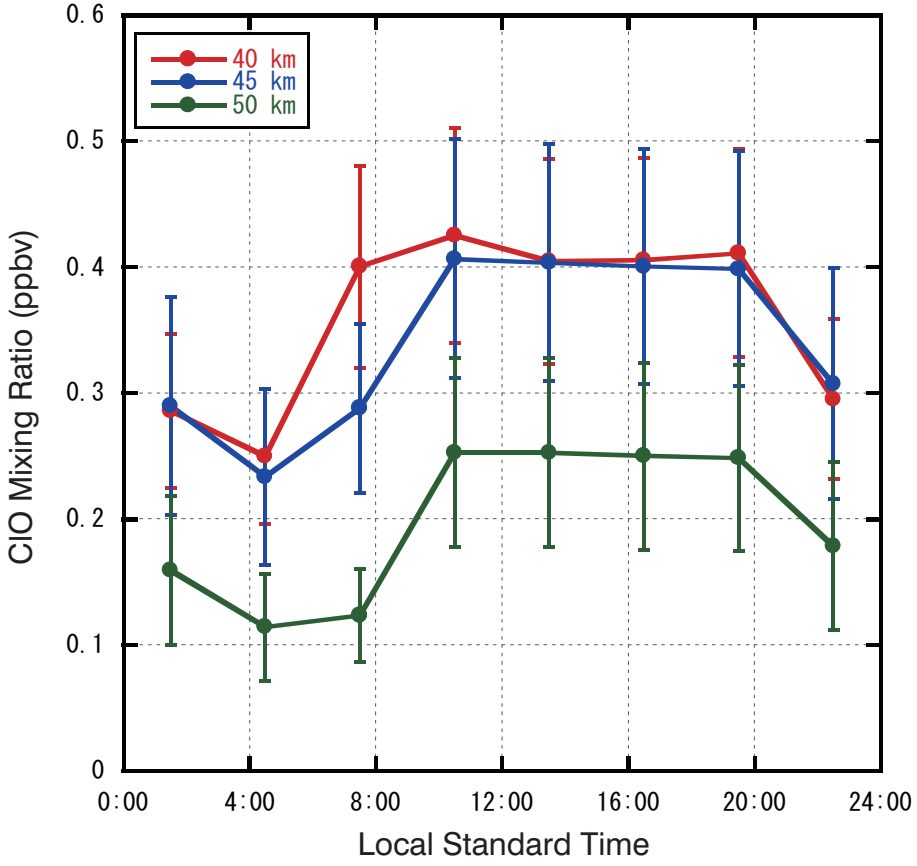

Fig. 13. Diurnal variations of ClO mixing ratio measured in from 5 to 16 December 2009. The red, blue and green line shows the diurnal variation at 40, 45 and 50 km, respectively.

AMTD
5, 1907–1945, 2012

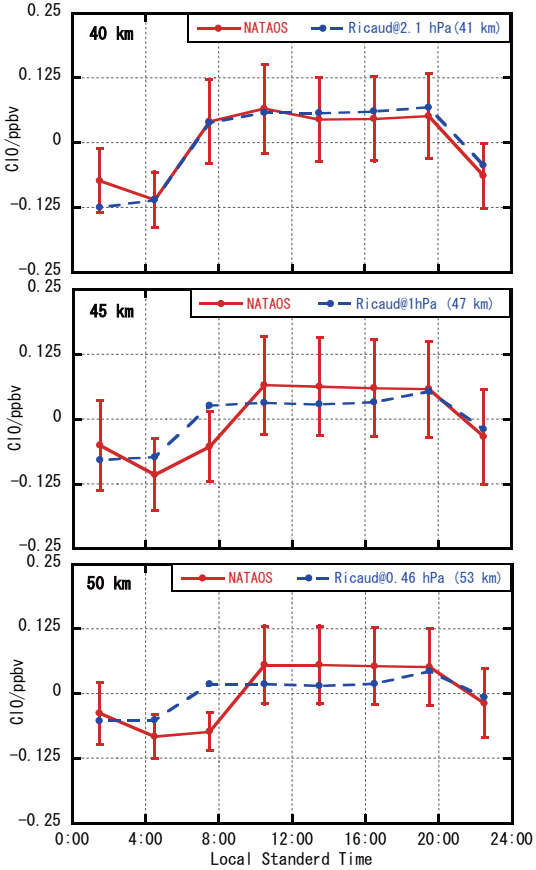

Fig. 14. The diurnal variations at (top) 40 km, (middle) 45 km and (bottom) 50 km as measured by out radiometer (red line). The blue line shows the diurnal variations estimated by the convolved UARS/MLS data measured from 1991 to 1997 within the band 40–50° N in July reported by Ricaud et al. (2000).

AMTD
5, 1907–1945, 2012